Title: S-acylation of the cellulose synthase complex is essential for its plasma membrane localization

Authors: Manoj Kumar[1], Raymond Wightman[2], Ivan Atanassov[1†], Anjali Gupta[1], Charlotte H. Hurst[3], Piers A. Hemsley[3]*, Simon Turner[1]*

Affiliations:

[1] University of Manchester; Faculty of Life Sciences; The Michael Smith Building; Oxford Road, Manchester M13 9PT, UK

[2] Microscopy Core Facility, Sainsbury Laboratory, University of Cambridge, Bateman Street, Cambridge. CB2 1LR, UK

[3] Division of Plant Sciences, School of Life Sciences, University of Dundee, Dow Street, Dundee, DD1 5EH, Scotland, UK

And

Cell & Molecular Sciences, The James Hutton Institute, Invergowrie, DD2 5DA, Scotland, UK.

[†] Present Address: AgroBioInstitute; 8 Dragan Tzankov Blvd; 1164 Sofia; Bulgaria

*Correspondence to: simon.turner@manchester.ac.uk, p.a.hemsley@dundee.ac.uk

Abstract: Plant cellulose microfibrils are synthesized by a process that propels the cellulose synthase complex (CSC) through the plane of the plasma membrane. How interactions between membranes and the CSC are regulated is currently unknown. Here we demonstrate that all catalytic subunits of the CSC, known as cellulose synthase A (CESA) proteins, are S-acylated. Analysis of Arabidopsis CESA7 reveals 4 cysteines in variable region 2 (VR2) and 2 cysteines at the carboxy-terminus (CT) as S-acylation sites. Mutating both the VR2 and CT cysteines permits CSC assembly and trafficking to the Golgi, but prevents localization to the plasma membrane. Estimates suggest that a single CSC contains more than 100 S-acyl groups that greatly increases the hydrophobic nature of the CSC and likely influences its immediate membrane environment.

One Sentence Summary: The large protein complex that spins out cellulose fibers creates its own hydrophobic environment.

Main Text:

Cellulose in plants is synthesized at the plasma membrane by the cellulose synthase complex (CSC) that contains at least 18 catalytic CESA protein subunits (*1*). The direction of CSC movement and the orientation of cellulose microfibril deposition is determined by cortical microtubules (*2*). Movement of the CSC through the plane of the plasma membrane is likely to cause severe disruption to the lipid bilayer (*3*) suggesting membrane partitioning of this process may be important. Here we describe the modifications of CESA proteins and demonstrate their importance to the functioning of the CSC.

S-acylation involves reversible addition of an acyl group, often palmitate or stearate, to a cysteine residue that can affect protein structure or localization (*4*). A recent study identified many S-acylated proteins in plants (*5*), including CESA1 and CESA3, which are essential for cellulose

2

synthesis in the primary cell wall (*6*). We used acyl-RAC assays (*7*) to confirm that CESA1 is S-acylated (Fig. S1) and show that CESA6 is also S-acylated (Fig. 1A). Furthermore, all 3 CESAs required for cellulose synthesis in the secondary cell wall, CESA4, CESA7 and CESA8, are S-acylated (Fig. 1A), demonstrating that S-acylation is a common feature of CESA proteins involved in cellulose synthesis in both primary and secondary cell walls.

CESA7 has 26 cysteines (Fig. S2A). In order to identify S-acylated cysteines, we mutated individual CESA7 cysteines to serines and tested their ability to complement the *cesa7^{irx3-1}* mutant. None of the 8 cysteines in the Zn finger domain (ZR) showed any significant complementation (Figs. 2A, S3, S4). The structure of the RING-type zinc-finger domain from CESA7 (PDB ID: 1WEO) shows that all 8 cysteines are involved in coordinating 2 zinc atoms, making them unlikely to be S-acylated. Consequently, we focused our subsequent analysis on other regions of CESA7. Two highly-conserved cysteines in the short C-terminus (Table S1) are also essential for CESA protein function (Fig. 2A). None of the remaining 16 single cysteine mutants showed a substantial effect on cellulose content (Fig. 2A).

A cysteine-rich region lies within variable region 2 (VR2) (*8*). The number of VR2 cysteines is conserved among orthologous CESAs from different species, but varies between paralogous CESAs (Table S1). There are 4 VR2 cysteines in CESA7 (Fig. S2) and mutating them individually has no effect on cellulose biosynthesis (Figs. 2A, C). We hypothesized that if VR2 is a site of CESA S-acylation, the remaining cysteines may support sufficient S-acylation for CESA7 function. Consequently, we mutated all 4 VR2 cysteines in CESA7 (VR2$_{C/S}$). The VR2$_{C/S}$ mutant

exhibited no complementation of $cesa7^{irx3-1}$ (Fig. 2C). Thus, the cysteines in this region appear to be functionally redundant.

Having identified the VR2 and CT cysteines as potential S-acylation sites, we proceeded to determine if these sites were S-acylated. We generated a mutant in which both CT cysteines were mutated ($CT_{C/S}$). The $CT_{C/S}$ mutant did not complement the $cesa7^{irx3-1}$ mutant (Fig. 2B). Using Acyl-RAC assays we consistently found that S-acylation was dramatically reduced in the $VR2_{C/S}$ mutant, although some signal remained. The $CT_{C/S}$ mutants exhibited a smaller decrease in S-acylation (Figs. 1B, C). We then constructed a mutant in which both the VR2 and CT cysteines were mutated ($VR2/CT_{C/S}$). The $VR2/CT_{C/S}$ mutant exhibited no complementation (Fig. 2B) and CESA7 S-acylation was effectively abolished (Figs. 1B, C), consistent with the hypothesis that both the VR2 and CT cysteines are S-acylated.

In order to determine if some of the VR2 cysteines were more important than the others, these cysteines were mutated in all possible double and triple combinations. All 10 of these double and triple VR2 cysteine mutants had a lower cellulose content than the single VR2 cysteine mutants (Fig. 2C), indicating that all 4 cysteines are important. In order to explore sequence specificity around the VR2 cysteines, we replaced the 6 amino acid long motif containing 4 cysteines of CESA7 with a motif from the same region of either CESA8 ($CESA7_{CESA8VRC}$) which contains only 3 cysteines, or CESA4 ($CESA7_{CESA4VRC}$), which contains 6 cysteines in a 12 amino acid long motif (Fig. S2B). The $CESA7_{CESA4VRC}$ construct complemented the $cesa7^{irx3-7}$ mutant but $CESA7_{CESA8VRC}$ did not (Figs. 2D, S3D). We also observed that wild type levels of CESA7 S-acylation were restored in $CESA7_{CESA4VRC}$ but only partially in $CESA7_{CESA8VRC}$ (Fig. S5).

4

Restoration of activity in CESA7$_{CESA4VRC}$ would suggest that the lack of acylation in the VR2$_{C/S}$ mutant is not a result of changes to protein conformation caused by mutating the cysteines in this region.

To investigate the effect of S-acylation on the trafficking of the CSC, we performed live cell imaging of CESA7 in developing xylem of intact roots (Fig. 3). During vessel differentiation, CSCs can be seen both moving around the cell in the Golgi, where they exhibit a characteristic ring-shaped morphology, and as transverse bands at the plasma membrane that correspond to sites of secondary cell wall deposition and cortical microtubule localization (*9, 10*). Using wild type YFP-CESA7, this banded pattern can be seen in single images, movie projections (Figs. 3A, C) and in movies (Movie S1) and co-localizes with bands of cortical microtubules (Fig. S6). In contrast, neither of the VR2$_{C/S}$ or CT$_{C/S}$ mutants exhibited the banded pattern (Figs. 3A, C, Movies S2, S3). Furthermore, we did not observe co-localization of CESA7 with cortical microtubules in the VR2$_{C/S}$ mutant (Fig. S6). The banded pattern of CESA7 localization is only apparent during later stages of vessel differentiation. At earlier stages, YFP-CESA7 is localized mainly within the Golgi resembling the patterns seen in the VR2$_{C/S}$ and CT$_{C/S}$ mutants. Similarly, mechanical perturbation of the seedlings during the imaging process can lead to a loss of the banded pattern. In plants that contained both CFP tagged wild type CESA7 and YFP tagged VR2$_{C/S,}$ we were able to see bands with CFP-CESA7, indicative of localization at the plasma membrane, but not with YFP-VR2$_{C/S}$ (Fig. 3B). While we always observed banding in the lines containing only the CFP-CESA7, banding was not observed in additional lines with high levels of YFP-VR2$_{C/S}$ expression indicating this construct has a dominant negative effect on CFP-CESA7 localization. Trafficking of the CSC to the plasma membrane is known to occur from the Golgi via particles known as

5

microtubule-associated cellulose synthase compartments (MASCs) or small CESA compartments (SmaCCs) (*11, 12*). We analyzed the movement of the Golgi and found no differences in trafficking dynamics between the wild type and either the CESA7 VR2$_{C/S}$ or CT$_{C/S}$ mutants (Fig. S7A). The imaging data is consistent with the hypothesis that the defective S-acylation of the VR2$_{C/S}$ mutant interferes with Golgi to plasma membrane trafficking of the CSC. In both the CESA7 VR2$_{C/S}$ and CT$_{C/S}$ mutants, we were able to observe particles that resemble MASCs (Fig. S7B), but using the intact root system, we were unable to track their movement or observe individual insertion events. Consequently we cannot exclude the possibility of S-acylation defective CSCs being transiently inserted into the plasma membrane and rapidly re-cycled or plasma membrane insertion occurring at a much-reduced rate. However, the absence of any discernible banded pattern in these mutants suggests that loss of CSC from the plasma membrane does not cause an accumulation of MASCs or Golgi below sites of cell wall deposition. In future it will be interesting to determine exactly what point the trafficking is defective in the acylation-deficient mutant and whether interactions between the MASC and microtubules or other markers for sites of cell wall deposition are altered.

To explore how the trafficking of CESA is altered in the S-acylation deficient mutant, we examined the interactions of CESA subunits, since mutations in one CESA protein can affect the association between the remaining CESAs in the complex (*13*). We used the tag on the VR2/CT$_{C/S}$ mutant to pull down CESA7 and found both CESA4 and CESA8 could be co-precipitated. This suggests that all 3 CESAs are still able to associate as part of a complex, even in the absence of normal CESA7 S-acylation (Fig. 4A). S-acylation of CESA4 and CESA8 remained intact in the CESA7 VR2/CT$_{C/S}$ mutant (Fig. 4B) indicating that an S-acylation defect in one subunit does not affect

6

the S-acylation states of the others. Acylation of membrane proteins often causes conformation changes that maybe be essential for targeting and/or interactions with other proteins (*4*), so while CESA proteins still associate in CESA7 VR2/CT$_{C/S}$ mutants, they potentially have altered confirmations that could affect the correct assembly of the CSC.

VR2 encompasses a region known as the class-specific region (CSR) (*8*). Modeling studies have suggested that the CSR loops away from the catalytic core making it a candidate for subunit interactions (*14*). S-acylation of VR2 cysteines would alter the conformational prediction for this region by placing the beginning of the CSR adjacent to the plasma membrane suggesting further structural data for this region is required. The acyl groups are likely to be inserted into the plasma membrane close to the transmembrane region, in a region that is occupied by BcsB in the BcsA/B crystal structure of bacterial cellulose synthase (*6, 14, 15*). One of the major differences between the way in which bacteria and plants make cellulose, is the mobile nature of the plant CSC, which must be able to move through the plane of the plasma membrane as it makes cellulose. We speculate that this process may be facilitated by the S-acylation of plant CESA proteins.

Up to 6 cysteines are likely to be S-acylated in each of CESA7, CESA4, and CESA8. Thus a functional CSC, with at least 18 CESA proteins, would contain more than 100 S-acyl groups. The hydrophobic nature of S-acylation can make some proteins resistant to solubilization even by ionic detergents such as SDS (*16*). S-acyl groups can be removed by treatment with dithiothreitol (DTT) (*17*), which also reduces aggregation of CESA proteins during SDS-PAGE (*18*). Using mass spectrometry we have only been able to identify VR2 peptides from DTT treated samples. The very high level of S-acylation and hydrophobicity of the CSC and/or the requirement for a

specialized membrane environment is likely to make the CSC susceptible to aggregation and may explain why it has not been possible to purify an intact, active CSC. While S-acylation is known to affect partitioning of proteins into membrane microdomains, it has also been suggested that the crowding of S-acyl groups within a membrane may actually facilitate the formation of lipid microdomains (*19*). The high level of S-acylation found in the CSC would make it a very good candidate for a protein complex capable of generating lipid microdomains that may facilitate the co-localization of proteins with similar properties. We note that a recent proteomic study of S-acylated proteins also identified the endoglucanase KORRIGAN, a known CESA binding protein (*5*).

References and Notes:

1. A. N. Fernandes *et al.*, Nanostructure of cellulose microfibrils in spruce wood. *Proc. Natl. Acad. Sci. USA* **108**, E1195-E1203 (2011).

2. A. R. Paredez, C. R. Somerville, D. W. Ehrhardt, Visualization of cellulose synthase demonstrates functional association with microtubules. *Science* **312**, 1491-1495 (2006).

3. F. Diotallevi, B. Mulder, The cellulose synthase complex: A polymerization driven supramolecular motor. *Biophys. J.* **92**, 2666-2673 (2007).

4. P. A. Hemsley, The importance of lipid modified proteins in plants. *New Phytol.* **205**, 476-489 (2015).

5. P. A. Hemsley, T. Weimar, K. S. Lilley, P. Dupree, C. S. Grierson, A proteomic approach identifies many novel palmitoylated proteins in Arabidopsis. *New Phytol.* **197**, 805-814 (2013).

6. M. Kumar, S. Turner, Plant cellulose synthesis: CESA proteins crossing kingdoms. *Phytochemistry* **112**, 91-99 (2015).

7. M. T. Forrester *et al.*, Site-specific analysis of protein S-acylation by resin-assisted capture. *J. Lipid Res.* **52**, 393-398 (2011).

8. C. E. Vergara, N. C. Carpita, Beta-D-glycan synthases and the CesA gene family: lessons to be learned from the mixed-linkage (1-->3),(1-->4)beta-D-glucan synthase. *Plant Mol. Biol.* **47**, 145-160 (2001).

9. R. Wightman, S. R. Turner, The roles of the cytoskeleton during cellulose deposition at the secondary cell wall. *Plant J.* **54**, 794-805 (2008).

10. Y. Watanabe *et al.*, Visualization of cellulose synthases in Arabidopsis secondary cell walls. *Science* **350**, 198-203 (2015).

11. E. F. Crowell *et al.*, Pausing of golgi bodies on microtubules regulates secretion of cellulose synthase complexes in Arabidopsis. *Plant Cell* **21**, 1141-1154 (2009).

12. R. Gutierrez, J. J. Lindeboom, A. R. Paredez, A. M. C. Emons, D. W. Ehrhardt, Arabidopsis cortical microtubules position cellulose synthase delivery to the plasma membrane and interact with cellulose synthase trafficking compartments. *Nat. Cell Biol.* **11**, 797-U743 (2009).

13. N. G. Taylor, R. M. Howells, A. K. Huttly, K. Vickers, S. R. Turner, Interactions among three distinct CesA proteins essential for cellulose synthesis. *Proc. Natl. Acad. Sci. USA* **100**, 1450-1455 (2003).

14. L. Sethaphong *et al.*, Tertiary model of a plant cellulose synthase. *Proc. Natl. Acad. Sci. USA* **110**, 7512-7517 (2013).

15. J. L. W. Morgan, J. Strumillo, J. Zimmer, Crystallographic snapshot of cellulose synthesis and membrane translocation. *Nature* **493**, 181-U192 (2013).

16. S. Monier, D. J. Dietzen, W. R. Hastings, D. M. Lublin, T. V. Kurzchalia, Oligomerization of VIP21-caveolin in vitro is stabilized by long chain fatty acylation or cholesterol. *FEBS Lett.* **388**, 143-149 (1996).

17. O. Batistic, N. Sorek, S. Schultke, S. Yalovsky, J. Kudla, Dual fatty acyl modification determines the localization and plasma membrane targeting of CBL/CIPK Ca2+ signaling complexes in Arabidopsis. *Plant Cell* **20**, 1346-1362 (2008).

18. Atanassov, II, J. K. Pittman, S. R. Turner, Elucidating the Mechanisms of Assembly and Subunit Interaction of the Cellulose Synthase Complex of Arabidopsis Secondary Cell Walls. *J. Biol. Chem.* **284**, 3833-3841 (2009).

19. S. S. A. Konrad, T. Ott, Molecular principles of membrane microdomain targeting in plants. *Trends Plant Sci.* **20**, 351-361 (2015).

20. I. Atanassov, I. Atanassov, J. P. Etchells, S. Turner, A simple, flexible and efficient PCR-fusion/Gateway cloning procedure for gene fusion, site-directed mutagenesis, short sequence insertion and domain deletions and swaps. *Plant Methods* **5**, 14 (2009).

21. M. Kumar, S. Turner, Protocol: a medium-throughput method for determination of cellulose content from single stem pieces of Arabidopsis thaliana. *Plant Methods* **11**, 46 (2015).

22. S. J. Clough, A. F. Bent, Floral dip: a simplified method for Agrobacterium-mediated transformation of Arabidopsis thaliana. *Plant J.* **16**, 735-743 (1998).

23. D. M. Updegraff, Semimicro determination of cellulose in biological materials. *Anal. Biochem.* **32**, 420-& (1969).

24. P. A. Hemsley, L. Taylor, C. S. Grierson, Assaying protein palmitoylation in plants. *Plant Methods* **4**, 2 (2008).

25. N. G. Taylor, S. Laurie, S. R. Turner, Multiple cellulose synthase catalytic subunits are required for cellulose synthesis in Arabidopsis. *Plant Cell* **12**, 2529-2539 (2000).

Acknowledgments:

Supplementary Materials:

Materials and Methods

Figs. S1-S8

Tables S1-S2

Movies S1-S3

References (20-25)

FIGURE LEGENDS

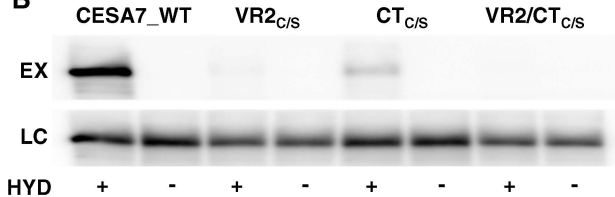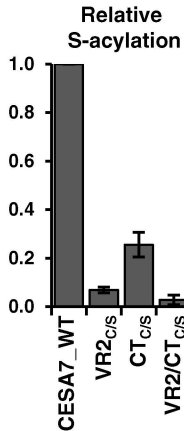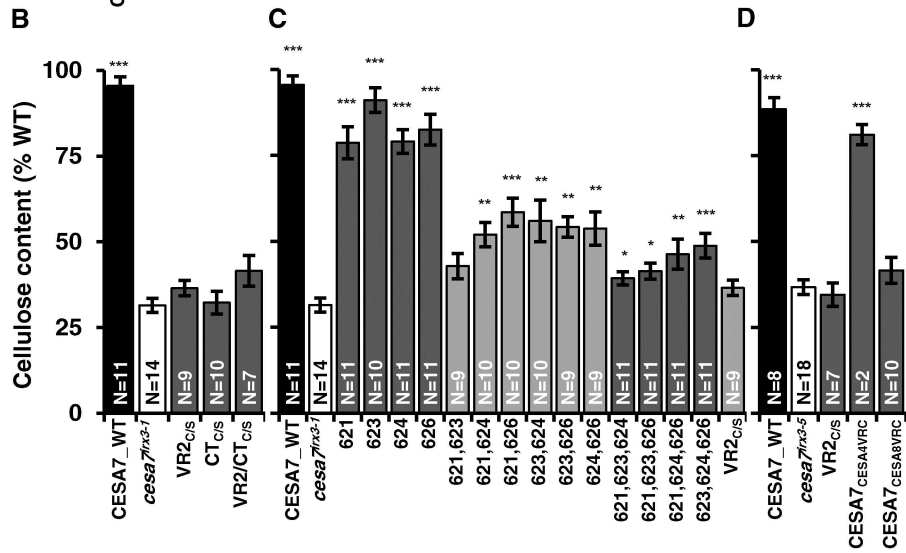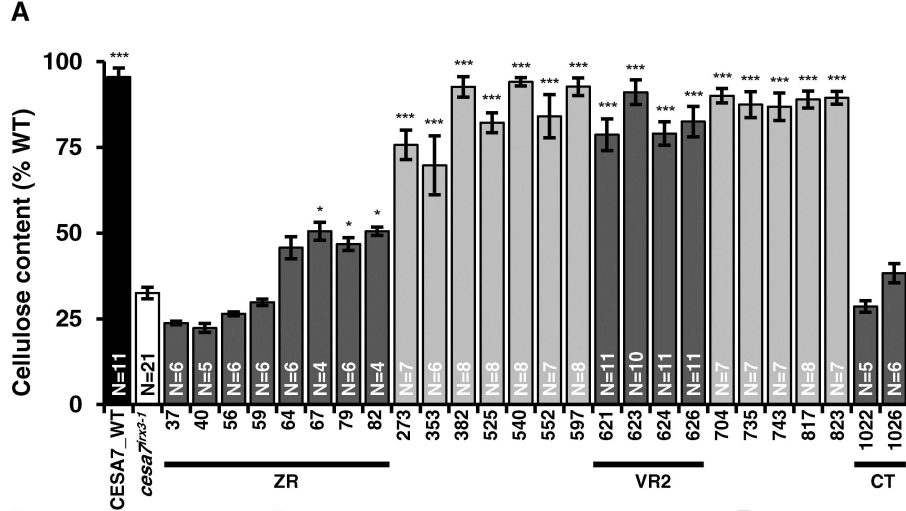**Fig. 1. Analysis of Arabidopsis CESA protein S-acylation.** S-acylation of various CESA proteins from WT plants assayed using biotin exchange or acyl-RAC assays (A) and CESA7 cysteine cluster mutants measured by acyl-RAC (B). For each assay, the experimental sample (EX) was compared with the loading control (LC) with or without (+/-) hydroxylamine (HYD) for hydroxylamine dependent capture of S-acylated proteins. Individual CESA proteins were detected with specific antibodies. (C) The genotypes shown in B were tested in 4 independent experiments. Relative levels of S-acylation are expressed a percentage of the wild type. Error bars represent SEM.
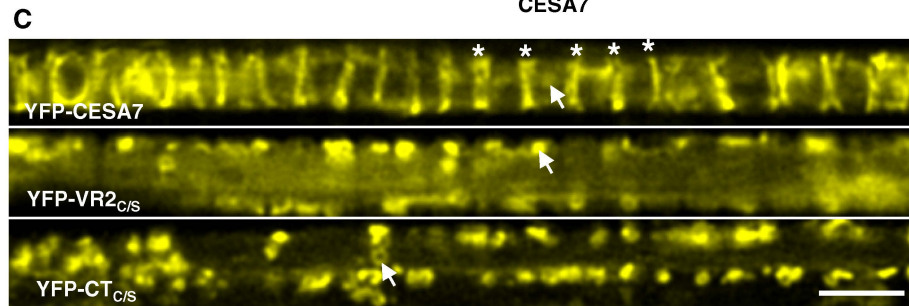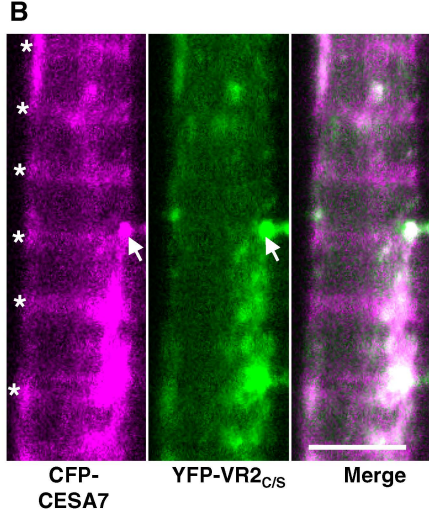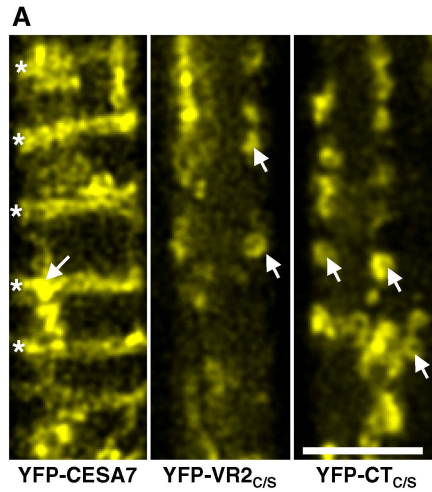
Fig. 2. Cellulose content of the CESA7 cysteine mutants. Cellulose content of single cysteine mutants (A), cysteine cluster mutants (B), VR2 cysteines mutant combinations (C), and mutants with CESA7 VR2 cysteines replaced with those of CESA4 and CESA8 (D) are shown. The numbers on the horizontal axis in panels A and C refer to the CESA7 residue number of the mutated cysteines. Zinc finger (ZR), variable region 2 (VR2) and C-terminus (CT) domains mentioned in text are highlighted with black lines in panel A. Cellulose content is expressed as percentage of the wild type using Landsberg erecta (Ler-0) for $cesa7^{irx3-1}$ (panel A, B, C) or Colombia (Col-0) for $cesa7^{irx3-7}$ (panel D). Error bars are SEM. Significance values are for comparison of each genotype to the mutant control in a univariate ANOVA test. Significance at 0.001***, 0.01** or 0.05 * levels are indicated.
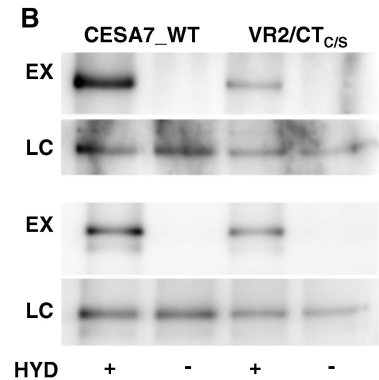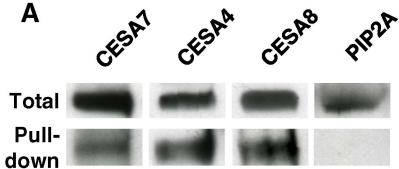
13

Fig. 3. Loss of acylation affects CSC localisation at the plasma membrane. In live cell imaging of the CSC in developing xylem vessels of intact roots using YFP-CESA7, CSCs at the plasma membrane appear as lateral bands (asterisk), whilst in the Golgi, CSCs are visualised as ring shaped particles (arrowheads). (A) Single frame images showing localisation of YFP tagged WT CESA7 and the VR2$_{C/S}$ and CT$_{C/S}$ mutants. (B) Single frame images showing CFP-CESA7 (magenta) and YFP-VR2$_{C/S}$ (green) within the same cell. (C) Average projections taken from movies showing YFP tagged WT CESA7 and the VR2$_{C/S}$ and CT$_{C/S}$ mutants. Scale bars are 5 µm.

Fig. 4. Loss of CESA7 acylation does not affect the CSC sub-unit association or S-acylation of other CESAs in the complex. (A) Total protein and Ni2+ affinity purified CESA7 samples from CESA7 VR2/CTC/S mutant were probed with the CESA antibodies indicated. PIP2 was used as a control. (B) S-acylation status of CESA4 (top) and CESA8 (bottom) was determined in CESA7_WT and CESA7 VR2/CTC/S plants using Acyl-RAC. For each assay the experimental samples (EX) were compared with the loading control (LC) with or without (+/-) hydroxylamine (HYD) for hydroxylamine dependant capture of S-acylated proteins. Blots were probed with either anti-CESA4 or anti-CESA8 specific antibodies.

A

	CESA8	CESA7	CESA4	CESA6
EX				
LC				
HYD	+ −	+ −	+ −	+ −

B

	CESA7_WT	VR2$_{C/S}$	CT$_{C/S}$	VR2/CT$_{C/S}$
EX				
LC				
HYD	+ −	+ −	+ −	+ −

C Relative S-acylation

A

YFP-CESA7   YFP-VR2$_{C/S}$ YFP-CT$_{C/S}$

B

CFP-CESA7   YFP-VR2$_{C/S}$ Merge

C

YFP-CESA7

YFP-VR2$_{C/S}$

YFP-CT$_{C/S}$

A

	CESA7	CESA4	CESA8	PIP2A
Total				
Pull-down				

B

	CESA7_WT	VR2/CT$_{C/S}$
EX		
LC		
EX		
LC		

HYD   +   –   +   –

Science
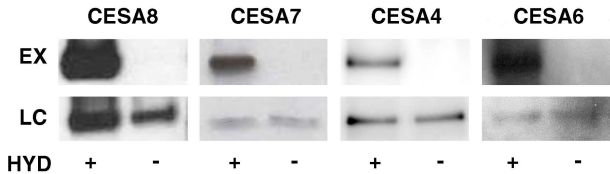
Supplementary Materials for

Extensive S-acylation of the cellulose synthase complex drives its plasma membrane integration

Manoj Kumar, Raymond Wightman, Ivan Atanassov, Anjali Gupta, Charlotte H. Hurst
Piers A. Hemsley, Simon Turner
correspondence to: simon.turner@manchester.ac.uk, p.a.hemsley@dundee.ac.uk

This PDF file includes:

> Materials and Methods
> Figs. S1-S8
> Tables S1-S2
> Captions for Movies S1-S3

Other Supplementary Materials for this manuscript includes the following:

> Movies S1 to S3

Materials and Methods

In Vitro mutagenesis

Basic principles of the mutagenesis technique have been described previously (*20*). Briefly, AtCESA7 was first cloned in pDONOR/Zeo (Invitrogen) by a BP clonase reaction to create an entry clone. For each mutant, 4 primers were designed: a general primer forward (GPF), a general primer reverse (GPR), a specific primer forward (SPF) and a specific primer reverse (SPR). PCR fragment A and B were amplified using a combination of GPF+SPR and SPF+GPR respectively. The sequences of GPF and GPR were GTTTTCCCAGTCACGACGTTGTAAAACGACGGCCAG and CAGGAAACAGCTATGACCATGTAATACGACTCACTA respectively. A list of all the specific primers used in the study is provided in Table S2. The PCR fragments were gel extracted and combined using an overlap extension reaction. The resulting product was purified again to remove unused reagents and used in an LR reaction along with a Gateway destination vector to produce expression clones under control of the AtCESA7 promoter. Gateway BP and LR reactions were carried out according to the manufacturer's instructions (Invitrogen). Transformants were selected on appropriate antibiotic selection. Plasmids were extracted from selected colonies and sequenced fully.

Three different Gateway destination vectors were constructed for this study, all based on pCambia background. The destination vector, VC05 was constructed based on pCambia2300 (kanamycin as plant selection) backbone. The component fragments – 1.7 kB CESA7 promoter, RGS-HIS-STREPII tag, the frame A (attR1/CmR/ccdB/attR2) Gateway cassette (Invitrogen) and the nitric-oxide synthase terminator from pGPTV-BAR (tNOS) were combined using restriction based cloning and overlap extension techniques.

This vector was used for all single and cluster mutants presented in Fig. 2A-C. VC02 was constructed in pCambia1300 (hygromycin as plant selection) backbone. This vector included all the components of VC05 except the RGS-HIS-STREPII tag and was used for the VR2 cysteine swaps presented in Fig. 2D. VC08 was constructed in pCambia1300 backbone. This vector uses RGS-HIS-STREPII-EYFP as the N terminal fusion tag and was used for the fluorescent constructs used in Fig. 4. To produce the VR2/CT$_{C/S}$ mutant, VR2$_{C/S}$ and CT$_{C/S}$ were first transferred into pDONOR/Zeo (Invitrogen). This was used as a template to produce the PCR fragments A and B, as described above, and cloned into VC05 destination vector using an LR clonase reaction.

Plant material and growth conditions

The *cesa7* mutants used in this study, *cesa7^{irx3-1}* and *cesa7^{irx3-7}*, have been described previously (*21*). All plasmids were transformed into Agrobacterium prior to Arabidopsis transformation using the floral dip method (*22*). T1 lines were selected on kanamycin (50 µg/mL) or hygromycin (35 µg/mL). After growing for 7 days on plates in an incubator, 8-10 independent lines for each construct were transplanted on a 1:1:5 mixture of perlite, vermiculite and compost. Plants were grown for a further 7 weeks on soil under long day conditions (16h/8h day/night, 22°C temperature). Plant height measurements were taken 7 weeks after sowing. After 7 weeks, a 50 mm piece from the primary inflorescence stem was harvested from 5 mm above the rosette level and stored in 70% ethanol for analysis of cellulose content. T2 seed was collected from the secondary inflorescences that were left intact. Plant growth and the cellulose content analysis was performed on the T1 and/or T2 generation.

Cellulose content determination

Stem material collected as described above was used for determination of cellulose content using a medium throughput adaptation of Updegraff's method (*21, 23*).

S-acylation assays

Multiple independent lines were tested for protein expression levels. Tissue was ground to a fine powder in liquid nitrogen before being solubilized in lysis buffer (100mM Tris pH 7.2, 150 mM NaCl, 25 mM EDTA, 2.5% SDS, with protease inhibitors). Protein was quantified by a BCA assay and 40 µg of protein was separated on a 7.5% SDS-PAGE gel before being transferred to a PVDF membrane for western blotting. Lines were selected from these analyses (Fig. S8). S-acylation assays were performed on the selected lines, essentially as described (*24*) but with modifications (*7*). Briefly, tissue was ground in liquid nitrogen and proteins were extracted in lysis buffer (100 mM Tris pH 7.2, 150 mM NaCl, 25 mM EDTA, 2.5% SDS, 25 mM N-ethylmaleimide with protease inhibitors), filtered through 2 layers or miracloth and centrifuged at 16k xg to remove insoluble debris. Protein concentrations were determined using a BCA assay. 2 mg of protein was made up to 1.5 ml in lysis buffer and incubated for 2 hours at RT with gentle mixing. Proteins were chloroform/methanol precipitated, briefly air dried and resuspended in 1 ml binding buffer (100 mM Tris pH 7.2, 150 mM NaCl, 25 mM EDTA, 2 % SDS, 6 M urea with protease inhibitors). Each sample was briefly centrifuged to remove insoluble precipitate and split in two. An equal volume of either 1 M hydroxylamine pH 7.2 (experimental) or 1 M NaCl (negative control) was added and mixed. 50 µl was removed as a loading control. To the

remaining sample 40 µl of a 50% suspension of thiopropyl sepharose CL-6b beads was added and incubated at RT for 1 hour. Beads were washed 3 times for 5 mins each with 1 ml binding buffer before being aspirated dry. Loading controls were chloroform/methanol precipitated after 1 hour incubation at RT. Beads and loading controls were resuspended in 20 µl 2x SDS page buffer containing 6 M urea and heated at 37°C for 30 mins with frequent mixing. Proteins were separated on a 7.5% SDS-PAGE gel and blotted to PVDF. Western blotting was performed using an anti-AtCESA4, 7 or 8 sheep polyclonal antisera as described (25).

Complex assembly assays

3 gram of stem material was ground to a fine powder in liquid nitrogen. 2.5 volumes of lysis buffer (50 mM Hepes, pH 7.5, 10 mM KCl, 300 mM Sucrose, 1 mM MgCl2) containing 20 mM Imidazole, 1 mM PMSF and 1X Protease Inhibitor Cocktail (Sigma) was added. After centrifugation at 600xg for 5 mins, Triton X-100 was added to make a final concentration of 1%. 120 µl of HisPur beads (Thermo Scientific) were added to the extract, which were mixed end-over-end for 2 hrs. After centrifugation, the resin was washed 4 times with 1 ml of lysis buffer containing 300 mM NaCl and 30 mM Imidazole. Protein was eluted from the resin 3 times with 300 µl of elution buffer (50 mM Hepes, pH 7.5, 300 mM NaCl and 250 mM Imidazole) and incubated with elution buffer for 10 mins at RT. 1X sample buffer containing 50 mM DTT was added to all eluates and heated at 65°C for 10 mins. The entire purification process was performed at 4°C unless mentioned otherwise. For preparing the loading control, 300 mg of stem material was directly prepared in 2.5 times of 1X sample buffer containing 50 mM DTT and heated at 65°C for 10 mins.

The loading controls and eluates were probed with CESA4, CESA7 and CESA8 (*13, 25*) and PIP-2s (from Agrisera) antibodies.

Confocal microscopy

Arabidopsis seedlings were prepared on slides for microscopy as previously reported (*9*). Imaging of root protoxylem was carried out on a Leica TCS SP8 confocal microscope (Leica Microsystems, UK) fitted with HyD SMD detectors and equipped with solid-state lasers 448 (for imaging CFP), 514 (for YFP) and 552 (for mCherry). A HC PL APO CS2 63x 1.4NA oil immersion objective was used with the zoom set to 2.4, unidirectional scanning set to speed 200 Hz and a line average of 3. The pinhole was set to 1.4 Airy units. To eliminate crossover, concurrent imaging of CFP and YFP was carried out using the line sequential mode. Deconvolution was carried out using Huygens (SVI, Netherlands) using verified metadata from the Leica LIF file format, with signal to noise ratios set to between 8 and 15 depending upon image quality, and output to a scaled 8-bit tiff format.
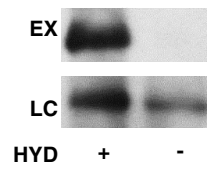
Fig. S1. Confirmation of CESA1 S-acylation. The experimental samples (EX) were compared with the loading control (LC) with or without (+/-) hydroxylamine (HYD) for hydroxylamine dependant capture of S-acylated proteins. Membranes were probed with anti-CESA1 antibody.
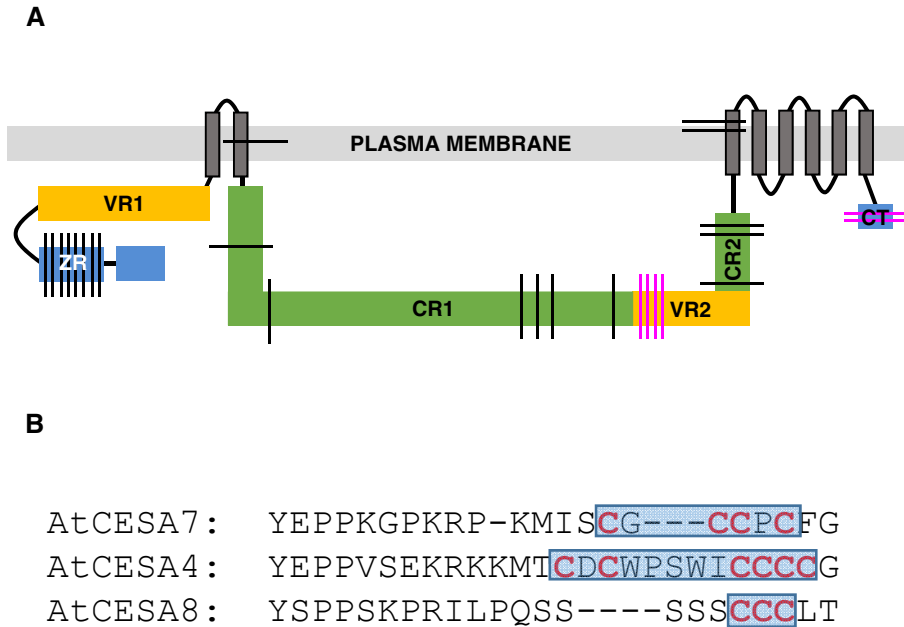
A

B

```
AtCESA7:  YEPPKGPKRP-KMISCG---CCPCFG
AtCESA4:  YEPPVSEKRKKMTCDCWPSWICCCCG
AtCESA8:  YSPPSKPRILPQSS----SSSCCCLT
```

Fig. S2. **Location of cysteines in CESA proteins.** (A) Diagrammatic representation of the position of cysteines within CESA7. The length of each labelled domain is proportional to their actual size. ZR (Zinc RING type finger), VR1 (variable region 1), CR1 (conserved region 1), VR2 (variable region 2), CR2 (conserved region 2) and CT (carboxy terminus) domains are shown. Cysteines are indicated by lines across the domains. The VR2 and CT cysteines referred to in the text are highlighted with magenta lines. (B) Part of the VR2 region of CESA4, 7 and 8 showing the number of VR2 cysteines in each protein. The sequences were taken from an alignment of the full length proteins made by CLUSTALX. Dashes represent gaps introduced by CLUSTAL to maximise the alignment. The shaded motif of CESA7 was replaced with the shaded motif in CESA4 and 8 to create CESA7$_{CESA4VRC}$ and CESA7$_{CESA8VRC}$ mutants respectively.
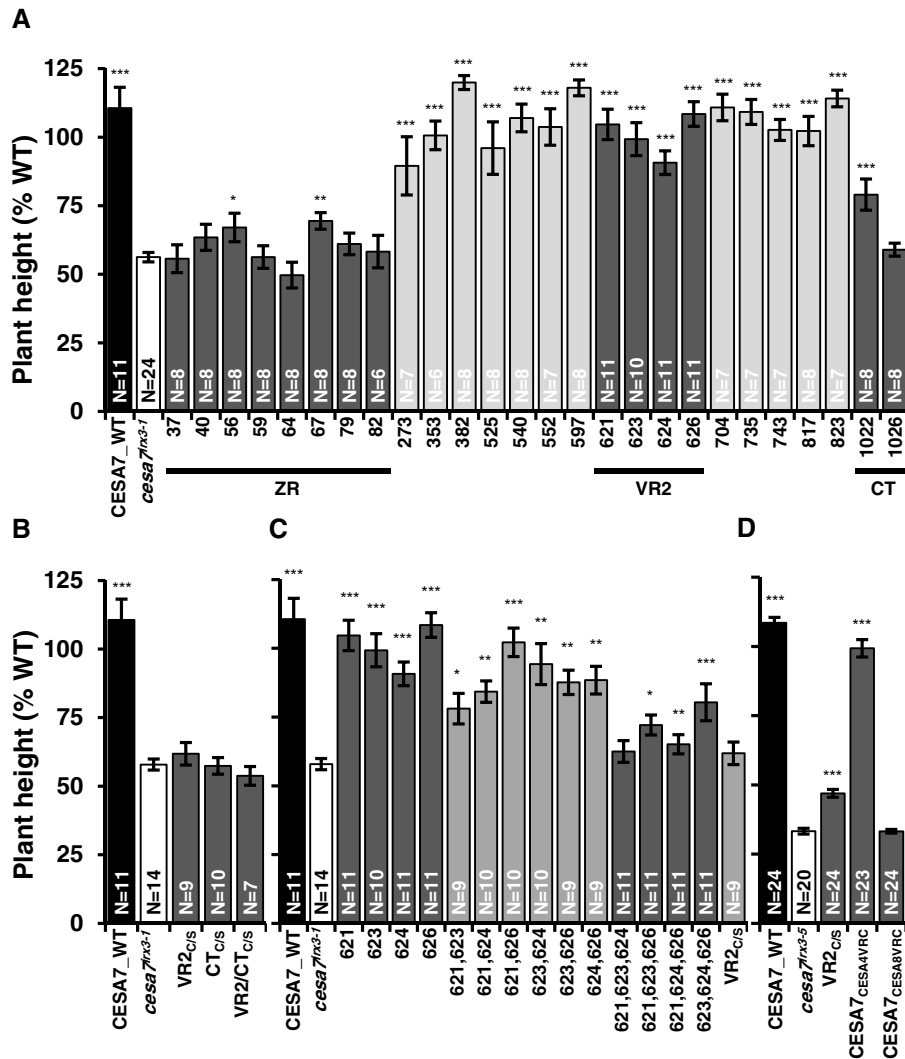
Fig. S3. **Growth analysis of the cysteine mutants.** Complementation of the plant height defect of *cesa7* mutants by single cysteine mutants (A), cluster mutants (B), VR2 cysteines mutant combinations (C) and mutants with CESA7 VR2 cysteines replaced with those of CESA4 and CESA8 (D) is shown. The numbers on the horizontal axis in panels A and C refer to the CESA7 amino acid residue number of mutated cysteines. Zinc finger (ZR), variable region 2 (VR2) and C-terminus (CT) domains mentioned in text are highlighted with black lines in panel A. Plant height is expressed as percentage of the wild type control. Ecotype backgrounds are Landsberg *erecta* (L*er*-0) for *cesa7irx3-1* (panel A, B, C) or Colombia (Col-0) for *cesa7irx3-7* (panel D). Error bars are SEM. Significance values are for comparison of each genotype to the mutant control in a univariate ANOVA test. Significance at 0.001***, 0.01** or 0.05 * levels are indicated.
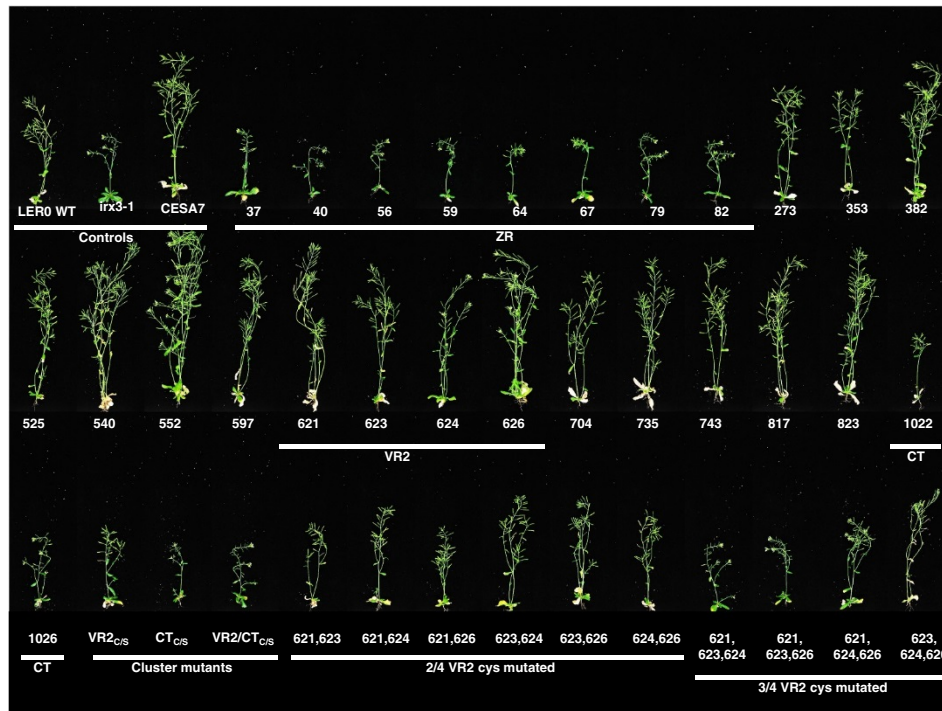
Fig. S4. Growth characteristics of cysteine mutants. Images were taken from representative plants at 41-days old. The numbers refer to the CESA7 amino acid residue of the mutated cysteines. Zinc finger (ZR), variable region 2 (VR2) and C-terminus (CT) domains mentioned in text are highlighted.
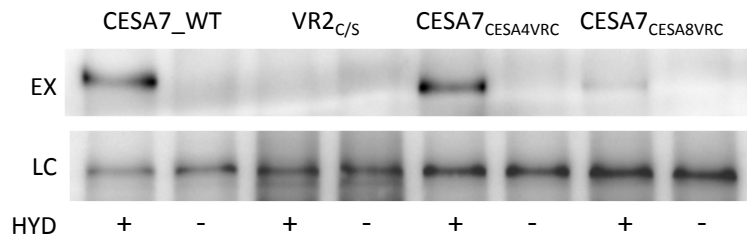
Fig. S5. Analysis of CESA7 acylation in the VR2 cysteine swaps. WT CESA7 and the VR2$_{C/S}$ mutant were transformed into *cesa7^{irx3-7}*. For the VR2 cysteine swaps, a 6 amino acid motif containing the VR2 cysteines in CESA7 was replaced with corresponding motif from CESA4 or CESA8 and transformed into *cesa7^{irx3-7}*. Acyl-RAC assays were performed on 8 day old seedlings. For each assay, the experimental samples (EX) was compared with the loading control (LC) with or without (+/-) hydroxylamine (HYD) for hydroxylamine dependent capture of S-acylated proteins. Samples were probed with anti-CESA7 antibodies.

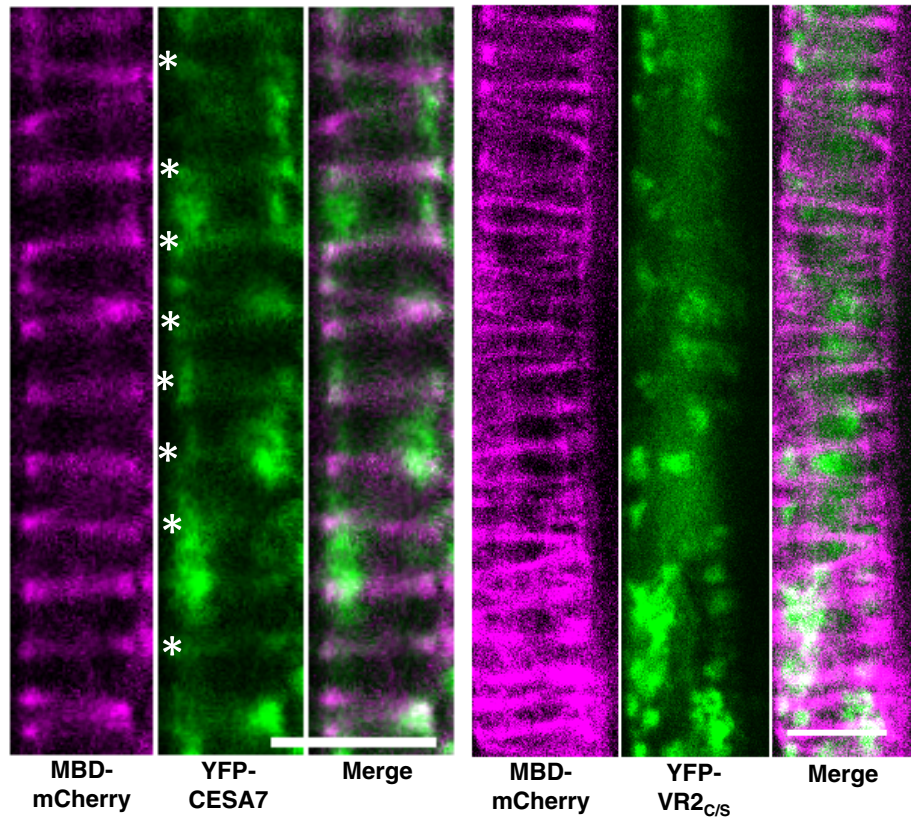**Fig. S6. Co-localisation of CESA7 with microtubules**. Microtubules were visualised with a pUBQ::MBD-mCherry reporter cassette (magenta) and the CSC with either pCESA7::YFP-CESA7 or pCESA7::YFP-VR2$_{C/S}$ (green). All scale bars are 5 μm.
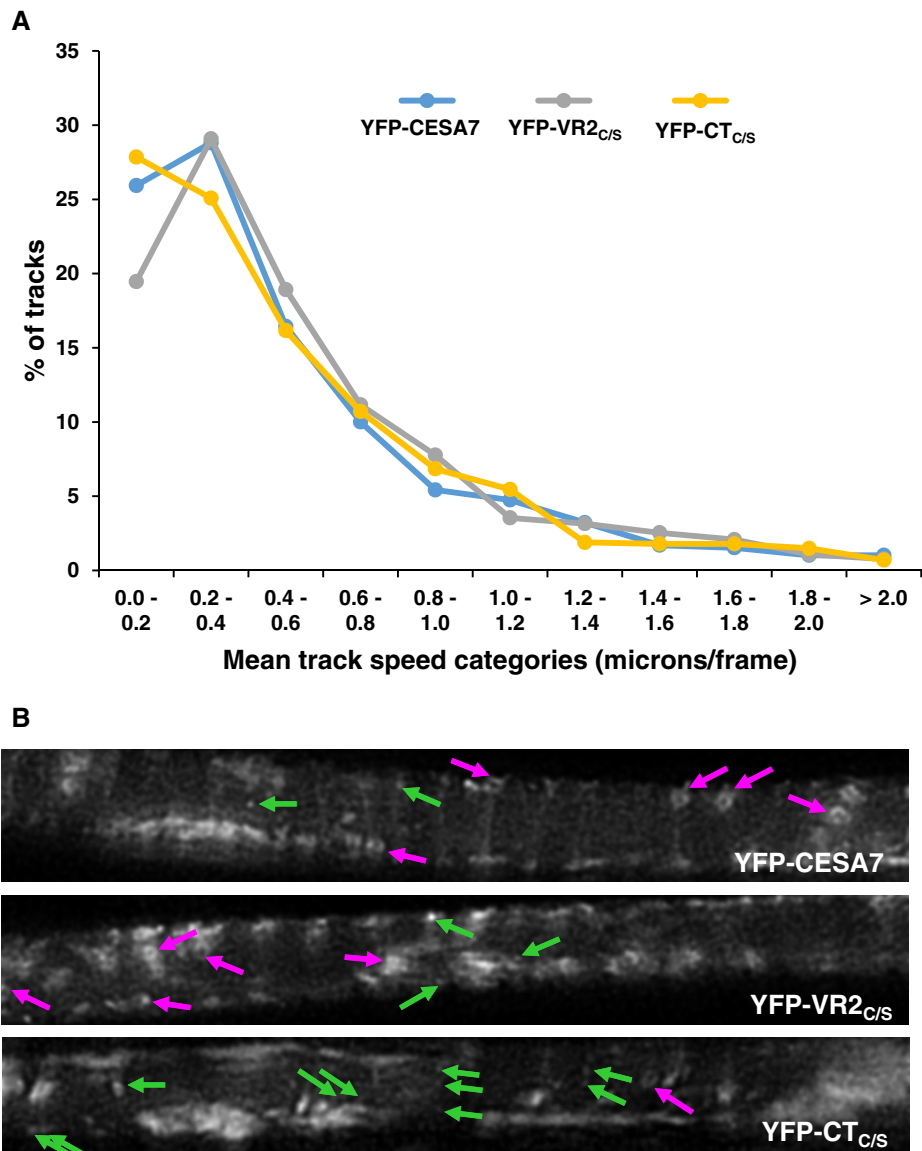
Fig. S7. Trafficking of the CSC in developing xylem vessels. (A) Time series movies were recorded for YFP-CESA7 (5 movies from 3 independent lines), YFP-VR2$_{C/S}$ (8 movies from 2 independent lines) and YFP-CT$_{C/S}$ (9 movies from 3 independent lines). Golgi particles were identified with the plugin TrackMate2 in Image J. Mean track speeds were calculated for all tracks for YFP-CESA7 (590 tracks), YFP-VR2$_{C/S}$ (1300 tracks), and YFP-CT$_{C/S}$ (1009 tracks). (B) Live cell imaging of the CSC in developing xylem vessels of intact roots performed using YFP-CESA7. The Golgi (magenta arrows) and MASC/SmaCCs (green arrows) are indicated. Localisation of YFP tagged WT CESA7 and the VR2$_{C/S}$ and CT$_{C/S}$ mutants is shown.
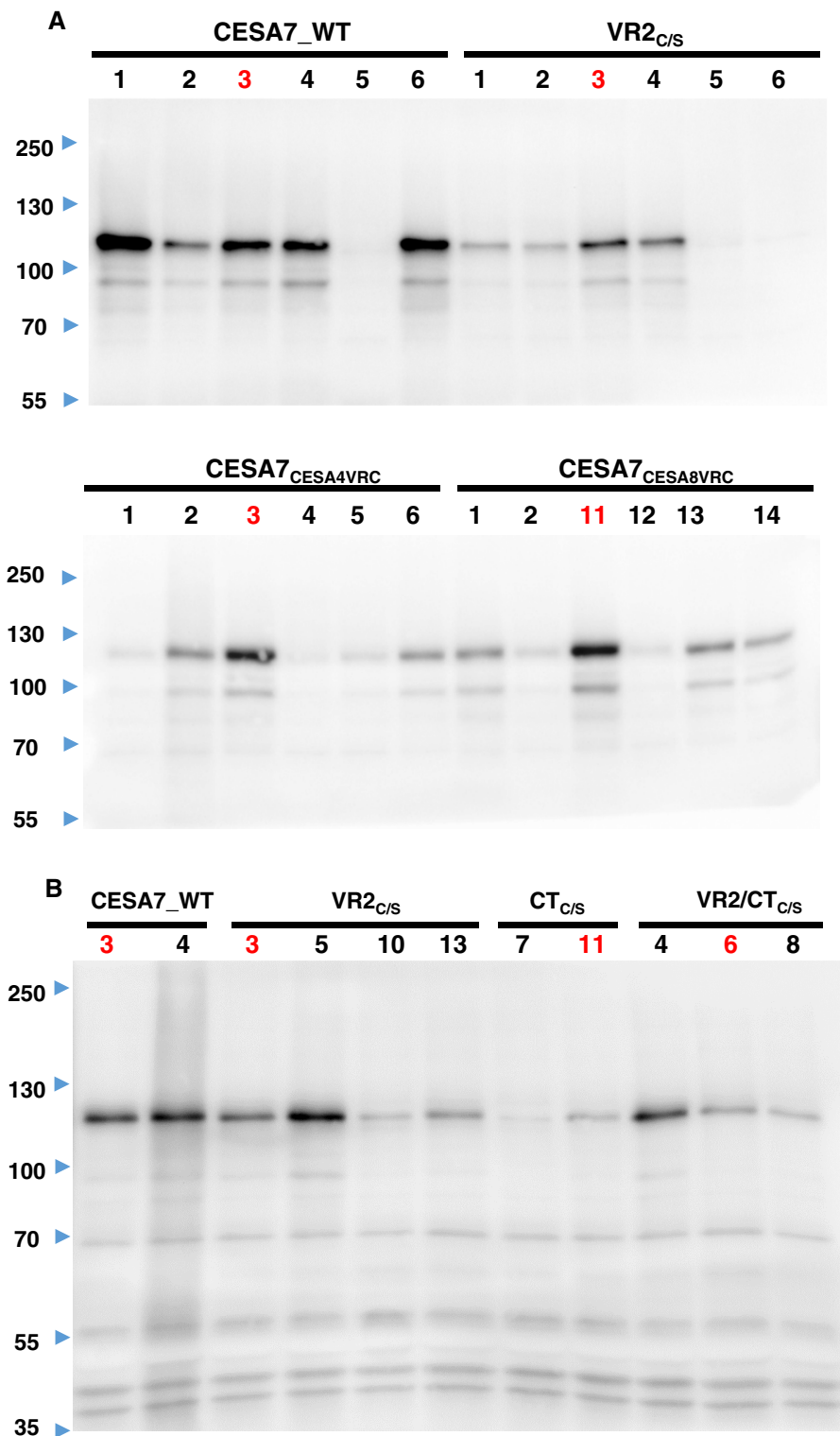
Figure S8. Protein expression analysis. Crude extracts containing 40 µg of total protein was loaded in each lane and probed with anti-CESA7 antibody. The numbers above each lane refers to the individual line numbers. The numbers in red indicate the lines used for S-acylation assays shown in Figs. S5 (A) and 1B (B). In panel A all lines were in the Colombia (Col-0) background using *cesa7irx3-7* while in panel B, the lines were in Landsberg *erecta* (L*er*-0) background using *cesa7irx3-1*.

Category (number of Cys)	CESA Class						
	CESA1	CESA3	CESA4	CESA6	CESA7	CESA8	CESA-Lower Plants
0	0	5	3	2	4	0	1
1	12	81	0	0	1	1	4
2	67	5	1	1	0	0	5
3	0	0	0	0	2	13	1
4	0	0	3	1	58	18	8
5	0	0	8	33	0	1	3
6	0	0	19	67	0	15	0
7	0	0	16	41	0	13	0
8	0	0	10	26	0	0	0
9	0	0	0	3	0	0	0
10	0	0	0	5	0	0	0
Total Proteins	79	91	60	179	65	61	22
Total Species	41	41	41	41	40	41	2
VR2 Cysteines							

Category (number of Cys)	CESA Class						
	CESA1	CESA3	CESA4	CESA6	CESA7	CESA8	CESA-Lower Plants
0	24	8	4	11	1	1	2
1	1	1	0	1	0	0	0
2	54	81	56	166	64	57	20
3	0	1	0	1	0	1	0
4	0	0	0	0	0	2	0
5	0	0	0	0	0	0	0
6	0	0	0	0	0	0	0
7	0	0	0	0	0	0	0
8	0	0	0	0	0	0	0
9	0	0	0	0	0	0	0
10	0	0	0	0	0	0	0
Total Proteins	79	91	60	179	65	61	22
Total Species	41	41	41	41	40	41	2
CT Cysteines							

Table S1. **Analysis of the number of VR2 and CT cysteines across plant genomes.** CESA families in 43 plant genomes were identified from Phytozome by BLAST searches against known CESA proteins from *Arabidopsis thaliana* and *Poplus trichocarpa*. All higher plant CESA proteins can be placed in one of the 6 classes (CESA1, 3, 6, 4, 7 and 8). These classes are named according to the Arabidopsis members of the class. CESAs from the lower plants, *Selaginella* and *Physcomitrella* form a distinct group by themselves (CESA-lower plants). After aligning the full length proteins from all species, the VR2 and CT regions were identified in the global alignment, the number of cysteines counted in each region and proteins were placed into cysteine number categories (0 to 10). The most abundant CESA class/Cys category combinations are highlighted in green. The total number of CESA proteins (and species) in each class are also shown. The 43 species involved in the analysis are: *Amborella trichopoda, Aquilegia coerulea, Arabidopsis halleri, Arabidopsis lyrata, Arabidopsis thaliana, Boechera stricta, Brachypodium distachyon, Brassica rapa FPsc, Capsella grandiflora, Capsella rubella, Carica papaya, Citrus clementina, Citrus sinensis, Cucumis sativus, Eucalyptus grandis, Eutrema salsugineum, Fragaria vesca, Glycine max, Gossypium raimondii, Linum usitatissimum, Malus domestica, Manihot esculenta, Medicago truncatula, Mimulus guttatus, Musa acuminata, Oryza sativa, Panicum hallii, Panicum virgatum, Phaseolus vulgaris, Physcomitrella patens, Populus trichocarpa, Prunus persica, Ricinus communis, Salix purpurea, Selaginella moellendorffii, Setaria italica, Solanum lycopersicum, Solanum tuberosum, Sorghum bicolor, Spirodela polyrhiza, Theobroma cacao, Vitis vinifera and Zea mays.*

Mutant Name	Mutated Cys	Specific Primer Forward (SFP)
$C^{37}S$	C37	ctagatggacaattcTCTgagatatgtggagatcag
$C^{40}S$	C40	caattctgtgagataTCTggagatcagattggtttta
$C^{56}S$	C56	gacctcttcgtagctAGCaatgagtgtggttttccg
$C^{59}S$	C59	gtagcttgcaatgagTCTggttttccggcgtgtaga
$C^{64}S$	C64	tgtggttttccggcgTCTagaccttgctatgagtac
$C^{67}S$	C67	ccggcgtgtagacctAGCtatgagtacgagagaaga
$C^{79}S$	C79	gaaggaacacaaaacTCTcctcagtgtaagactcgt
$C^{82}S$	C82	caaaactgtcctcagTCTaagactcgttacaagcgt
$C^{273}S$	C273	ctgacctctgtgatcTCTgaaatctggttcgctgtc
$C^{353}S$	C353	gttgagaaaatctccAGCtatgtctctgacgacggt
$C^{382}S$	C382	aaatgggttcccttcTCTaagaaattctccatagag
$C^{525}S$	C525	atgctgaacttggacTCTgatcactatgtaaacaac
$C^{540}S$	C540	gtgagggaagcaatgTCTttttttgatggatcctcag
$C^{552}S$	C552	attggaaagaaggtcAGCtatgttcagttccctcaa
$C^{597}S$	C597	tacgttggtactggtTCTgttttcaaacgacaagct
$C^{621}S$	C621	ccaaagatgataagcTCTggttgttgtccttgcttt
$C^{623}S$	C623	atgataagctgtggtTCTtgtccttgctttgggcgc
$C^{624}S$	C624	ataagctgtggttgtTCTccttgctttgggcgccgg
$C^{626}S$	C626	tgtggttgttgtcctAGCtttgggcgccggagaaag
$C^{704}S$	C704	atccatgtcataagcAGCggttatgaagacaagact
$C^{735}S$	C735	ggattcaagatgcatAGCcgtggatggaggtctatt
$C^{743}S$	C743	tggaggtctatttacAGCatgcctaagaggcctgca
$C^{817}S$	C817	ccacttcttgcctacTCTatccttccagccatctgt
$C^{823}S$	C823	atccttccagccatcTCTctccttactgacaaattc
$C^{1022}S$	C1022	cctgacacttccaagTCTggcatcaactgctgaagc
$C^{1026}S$	C1026	aagtgtggcatcaacAGCtgaagcaaaatctttttc
VR2$_{C/S}$	C621,C623,C624,C626	atgataagcTCTggtTCTTCTcctAGCtttgggcgc
CT$_{C/S}$	C1022,C1026	acttccaagTCTggcatcaacAGCtgaagcaaaatc
VR2/ CT$_{C/S}$	C621,C623,C624,C626, C1022,C1026	Forward tgccaacacaacaatctaccccttc Reverse ccgctccatctcaattccaagattc
$C^{621,623}S$	C621,C623	atgataagcTCTggtTCTtgtccttgctttgggcgc
$C^{621,624}S$	C621,C624	atgataagcTCTggttgtTCTccttgctttgggcgc
$C^{621,626}S$	C621,C626	atgataagcTCTggttgttgtcctAGCtttgggcgc
$C^{623,624}S$	C623,C624	atgataagctgtggtTCTTCTccttgctttgggcgc

C^{623,626}S	C623,C626	atgataagctgtggtTCTtgtcctAGCtttgggcgc
C^{624,626}S	C624,C626	atgataagctgtggttgtTCTcctAGCtttgggcgc
C^{621,623,624}S	C621,C623,C624	atgataagcTCTggtTCTTCTccttgctttgggcgc
C^{621,623,626}S	C621,C623,C626	atgataagcTCTggtTCTtgtcctAGCtttgggcgc
C^{621,624,626}S	C621,C624,C626	atgataagcTCTggttgtTCTcctAGCtttgggcgc
C^{623,624,626}S	C623,C624,C626	atgataagctgtggtTCTTCTcctAGCtttgggcgc
CESA7$_{CES}$ A4VRC	NA	atgacatgtgattgttggccgtcgtggatctgctgttgtt gcggcggaggtaaccgtaatagaaagaataag
CESA7$_{CES}$ A4VRC	NA	attttaccgcaatcttcatcatcgtcgtgttgctgtctaac caagaagagaaagaataag

Table S2. Sequence of primers used for mutagenesis. Mutated codons are indicated by upper case letters. VR2/CT$_{C/S}$ was made by combing the VR2 $_{C/S}$ and CT$_{C/S}$ mutants using the primers indicated. Unless indicated, the sequences of Specific Primer Reverse (SPR) are reverse compliment of the Specific Primer Forward sequences.

Movie S1.
Time course movie of YFP-CESA7 in a developing xylem vessel in the root of an Arabidopsis seedling.

Movie S2.
Time course movie of YFP-VR2$_{C/S}$ in a developing xylem vessel in the root of an Arabidopsis seedling.

Movie S3.
Time course movie of YFP-CT$_{C/S}$ in a developing xylem vessel in the root of an Arabidopsis seedling.